Available online at www.sciencedirect.com
ScienceDirect
Continental Shelf Research 27 (2007) 20–42
CONTINENTAL SHELF RESEARCH
www.elsevier.com/locate/csr

Tidal effects on estuarine circulation and outflow plume in the Chesapeake Bay

Xinyu Guo[a,*], Arnoldo Valle-Levinson[b]

[a]Center for Marine Environmental Studies, Ehime University, 2-5 Bunkyo-Cho, Matsuyama 790-8577, Japan
[b]Department of Civil and Coastal Engineering, University of Florida, 365 Weil Hall, P.O. Box 116580, Gainesville, FL 32611, USA

Received 10 January 2006; received in revised form 17 August 2006; accepted 30 August 2006
Available online 1 November 2006

Abstract

The response of the Chesapeake Bay to river discharge under the influence and absence of tide is simulated with a numerical model. Four numerical experiments are examined: (1) response to river discharge only; (2) response to river discharge plus an ambient coastal current along the shelf outside the bay; (3) response to river discharge and tidal forcing; and (4) response to river discharge, tidal forcing, and ambient coastal current. The general salinity distribution in the four cases is similar to observations inside the bay. Observed features, such as low salinity in the western side of the bay, are consistent in model results. Also, a typical estuarine circulation with seaward current in the upper layer and landward current in the lower layer is obtained in the four cases. The two cases without tide produce stronger subtidal currents than the cases with tide owing to greater frictional effects in the cases with tide. Differences in salinity distributions among the four cases appear mostly outside the bay in terms of the outflow plume structure. The two cases without tide produce an upstream (as in a Kelvin wave sense) or northward branch of the outflow plume, while the cases with tide produce an expected downstream or southward plume. Increased friction in the cases with tide changes the vertical structure of outflow at the entrance to the bay and induces large horizontal variations in the exchange flow. Consequently, the outflow from the bay is more influenced by the bottom than in the cases without tide. Therefore, a tendency for a bottom-advected plume appears in the cases with tide, rather than a surface-advected plume, which develops in the cases without tide. Further analysis shows that the tidal current favors a salt balance between the horizontal and vertical advection of salinity around the plume and hinders the upstream expansion of the plume outside the bay.

Keywords: Estuarine dynamics; River plume; Tidal effects; Vertical mixing; Mathematical models; Chesapeake bay

1. Introduction

Studies on the circulation and salinity distributions in Chesapeake Bay have a long history (Pritchard, 1952). Using observations, (Pritchard, 1954, 1956) constructed a two-dimensional (2D) framework for the dynamics of estuarine circulation, in which the effects of tidal currents on the salt and momentum balances in an estuary were recognized. Boicourt (1973) depicted the nature of the Chesapeake Bay outflow plume and the intruding oceanic flow underneath. Goodrich and Blumberg (1991) demonstrated the presence of an estuarine circulation in the Chesapeake Bay based on 168 current records from 1977 to 1983.

*Corresponding author. Tel./fax: +81 89 927 9824.
E-mail address: guoxinyu@dpc.ehime-u.ac.jp (X. Guo).

0278-4343/$ - see front matter © 2006 Elsevier Ltd. All rights reserved.
doi:10.1016/j.csr.2006.08.009

This consisted of a seaward current in the surface layer and a landward current in the lower layer. Observations across the entrance to the Chesapeake Bay showed that the exchange flow varies largely in the transverse direction (Valle-Levinson et al., 1998). An analytical solution illustrated that not only bathymetry variations but also friction is crucial to determine the transverse structure of exchange flows across the entrance to any estuary (Valle-Levinson et al., 2003). Following these observational and theoretical studies, the circulation in the Chesapeake Bay at any time scale should be studied in a 3D framework. Such framework should include a realistic bathymetry and tidal forcing.

Numerical simulations on the estuarine circulation in Chesapeake Bay also have a long history. Using a 3D primitive equation numerical model, Chao and Boicourt (1986) carried out a pioneering simulation of a plume in an idealized estuary with an adjacent shelf ocean. With a very similar model, Chao (1988a, b, 1990) investigated the influences of the bottom slope, winds and tide on the plume. Concentrating on the water exchange at the Chesapeake Bay entrance, Valle-Levinson et al. (1996) studied numerically the dynamics at the transition between an idealized estuary and an adjacent shelf. Wheless and Valle-Levinson (1996) investigated intratidal variations of a plume in an idealized inlet-shelf domain. Several numerical simulations with bathymetries that resemble those of Chesapeake Bay have also been carried out. Spitz and Klinck (1998) simulated the tides in the Chesapeake Bay by assimilating data from tide gauges. Wang and Johnson (2000) developed a 3D hydrodynamic model for the Chesapeake Bay, in which the model was driven by realistic forcing from 1985 to 1994. Xu et al. (2002) demonstrated the improvements of model results by assimilating high-resolution salinity data. Recently, Li et al. (2005) applied Regional Ocean Modeling System (ROMS) to the Chesapeake Bay and examined the sensitivity of model results to turbulence mixing parameterizations. At present, several other 3D numerical models for this estuary are being developed (http://ccmp.chesapeake.org/CCMP/workshops.html).

In this study, a 3D numerical model is used to examine the effects of tidal currents on estuarine circulation in Chesapeake Bay. Because of important effects of bathymetry in the bay (Valle-Levinson et al., 2003), a fine grid size (~400 m) is implemented in the simulations. Fresh water discharge, tidal forcing, and ambient coastal current outside the bay are used to drive the model. By including and excluding tidal forcing and ambient coastal currents, their effects on the subtidal currents are examined inside and outside the bay.

After a description of the numerical model in Section 2, the model results for the four cases are shown in Section 3. Analysis of the dynamics of the plume outside the bay is given in Section 4 along with a comparison with other studies. Finally, a summary is given in Section 5.

2. Numerical model

One of the community ocean models, the Princeton Ocean Model (POM), is used as the basic model. The POM is a 3D primitive equation ocean model that includes full thermodynamics and a level 2.5 Mellor–Yamada turbulence closure model (Blumberg and Mellor, 1987; Mellor, 1998). The model domain and bathymetry are shown in Fig. 1. The horizontal resolution is $1/240^\circ$ in both the zonal and meridional directions. In the vertical, 11 sigma-levels are evenly arranged. The minimum water depth in the model domain is set to 3 m. The time step is 3 s for the external mode and 120 s for the internal mode. During the calculations, the vertical eddy viscosity and diffusivity are given by the Mellor–Yamada turbulence closure model with a background value of $10^{-5}\,m^2/s$. The horizontal eddy viscosity is calculated by the embedded Smagorinsky formula with a proportionality parameter of 0.1, and the horizontal eddy diffusivity is obtained using an inverse Prandtl number of 0.5.

At the surface, no wind stresses are imposed. The bottom stresses (τ_x, τ_y) are calculated using a quadratic friction law:

$$(\tau_x, \tau_y) = \rho C_z(u, v)(u^2 + v^2), \tag{1}$$

where ρ is the water density, u and v are zonal and meridional components of velocity. The bottom drag coefficient is calculated by the embedded formula in POM (Mellor, 1998),

$$C_z = \max\left(0.0025, \frac{\kappa^2}{[\ln(0.05H/z_0)]^2}\right), \tag{2}$$

where $\kappa = 0.4$ is the von Karman constant, H the water depth, and z_0 the roughness parameter that is set to 0.1 cm.

The model is forced with river discharge, ambient coastal current and tides. The water temperature is set as a constant ($= 15^\circ$) and only the salinity is solved. Instead of using the standard central difference scheme for tracer advection, we used the

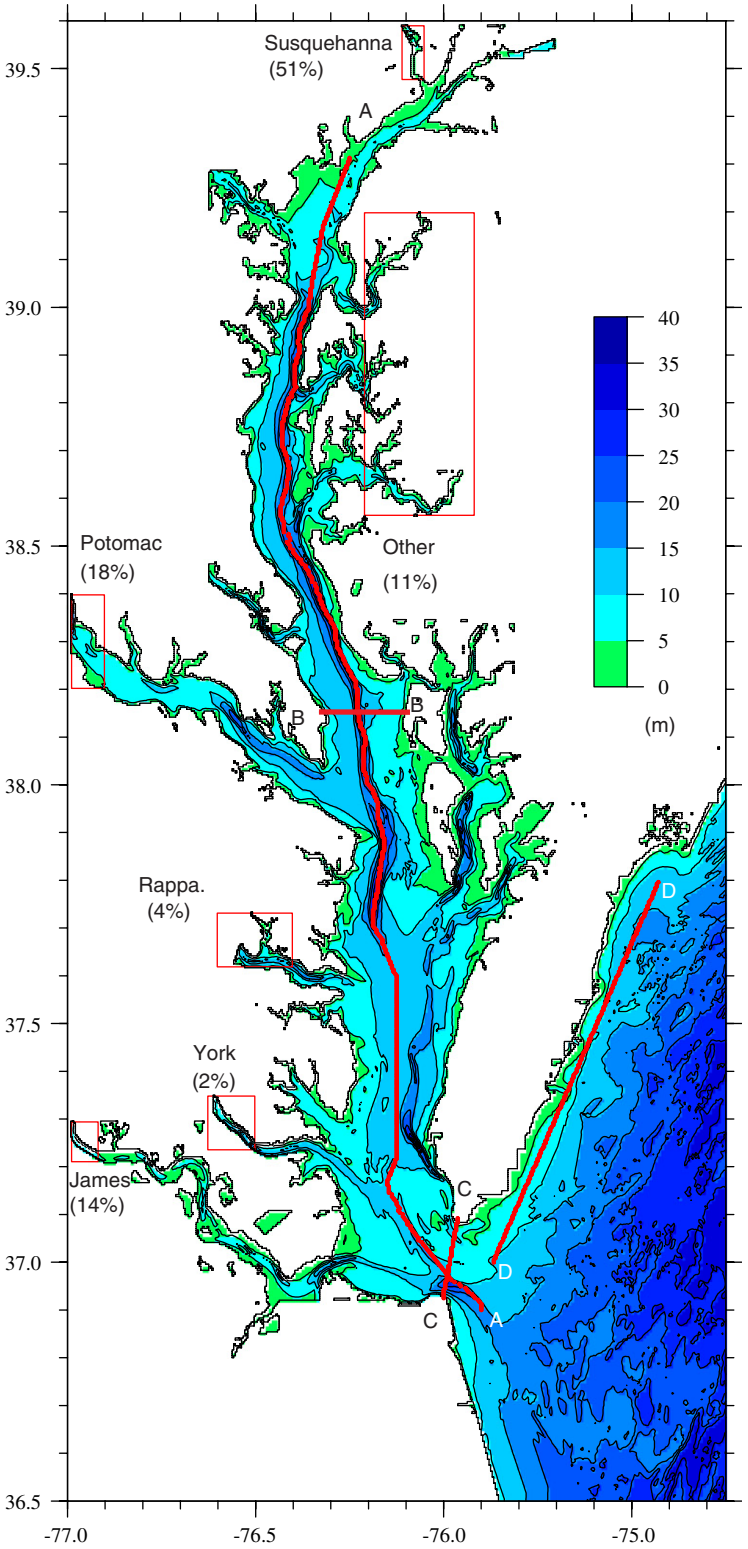

Fig. 1. Model bathymetry. The boxes denote location of rivers and the numbers inside the parentheses denote the ratio of river discharge of each river to total river discharge, which are given by Hargis (1980). Four red lines denote location of four sections shown in subsequent figures.

Smolarkiewicz iterative upstream scheme (Smolarkiewicz, 1984). This scheme has been included in the code of POM. Comparison of results calculated by the central difference scheme and by the Smolarkiewicz scheme showed that the Smolarkiewicz scheme produced a sharper river plume outside the Chesapeake Bay than the central difference scheme (figures not shown here).

Referring to Hargis (1980), a total of 2200 m^3/s of fresh water is introduced into the model domain from the Susquehanna (51% of total), Potomac (18%), James (14%), Rappahannock (4%), York (2%), and the other small rivers (11%)(see Fig. 1 for the position of the rivers). The river input is distributed to the corresponding grid points shown in Fig. 1 by specifying the vertical velocity $w_s = -Q/(N\Delta x\Delta y)$ (Oey, 1996), where Q is river discharge (m^3/s), N is the number of grid points covered by the river head and Δx and Δy are the sizes of grid points in the east and north directions, respectively. The salinity of river water is assumed to be 0 psu.

Prescription of the southward ambient current in the shelf was motivated by previous studies. Beardsley and Boicourt (1981) reported a southward coastal current in the Middle Atlantic Bight. Epifanio and Garvine (2001) presented the horizontal distribution of the coastal current south of Delaware Bay and inferred the existence of a southward coastal current outside the Chesapeake Bay. In our simulations, we impose an ambient coastal current with a speed of 10 cm/s along the eastern boundary from 37.7 to 38 °N.

The M_2 tide is the dominant tidal constituent in the Chesapeake Bay (Browne and Fisher, 1988; Shay et al., 2001). It is introduced in the simulations through oscillation of tidal currents along the eastern and southern boundaries. The harmonic constants of tidal currents along the eastern and southern boundaries are calculated in advance using a horizontal 2D model in which the oscillation of sea level is imposed. The amplitude and phase of the M_2 tide along the eastern and southern boundaries are 46 cm and 210°, which produce similar calculated tidal charts to observations in the entire Chesapeake Bay (Browne and Fisher, 1988).

The open boundary conditions are specified in the same way as in the subroutine BCOND in POM. In the case that includes both tidal currents and ambient current, a linear superposition of the two currents at the open boundary is used.

In this study, four cases are compared. In the first case (Case 1), only river discharge is introduced; in the second case (Case 2), river discharge and ambient coastal current are included; in the third case (Case 3), river discharge and the M_2 tide are prescribed; and in the fourth case (Case 4), river discharge, ambient coastal current, and the M_2 tide are introduced. All the simulations start from rest with an initial salinity of 32 psu at all grid points and run for 360 days. The results of Cases 3 and 4 are saved hourly and the tidal components are removed with a tide killer filter (Hanawa and Mitsudera, 1985).

Before examining subtidal currents, we confirmed the reproduction of adequate M_2 tide and tidal current distributions by the model. The amplitude of the M_2 tide (Fig. 2a) shows the same features as those from observations (Fig. 17 in Browne and Fisher, 1988) and results of data assimilation (Fig. 10 in Spitz and Klinck, 1998). Its amplitude is slightly lower along the western coast than along the eastern coast of the bay, which is attributed to Earth's rotation effects (Browne and Fisher, 1988). Two regions with the lowest amplitude are found around 37.6°N and 38.8°N along the western coast and are related to virtual amphidromic points. The phase of the M_2 tide (Fig. 2b) varies more than one tidal cycle from the mouth to the head of the bay, which is consistent with observations (Fig. 15 in Browne and Fisher, 1988) and results of data assimilation (Fig. 11 in Spitz and Klinck, 1998). The M_2 tidal current amplitude (Fig. 3a) is largest in the lower bay and at two other areas: the junction of the Potomac River and Chesapeake Bay and in the upper bay near Annapolis in the vicinity of the Bay Bridge. The features shown in these distributions, as well as the values of the M_2 tidal current amplitude, are consistent with observations (Browne and Fisher, 1988; Shay et al., 2001). The phase of the M_2 tidal current (Fig. 3b) increases from the mouth to the head of the bay and is similar to the distribution of the tidal elevation phase. The effect of friction on the tidal current is shown in Fig. 3b. The smaller value of phase near the coast than in the central part of the Chesapeake Bay results from relatively stronger friction over the shallow water with respect to deep water. As for the vertical structure of tidal current (not shown here), the modeled tidal current at the entrance to the bay weakens near the bottom and over shoals, which is consistent with observations by Valle-Levinson et al. (1998). All of these comparisons suggest that the calculated tides and tidal currents have satisfactory characteristics for examining tidal effects on estuarine circulation.

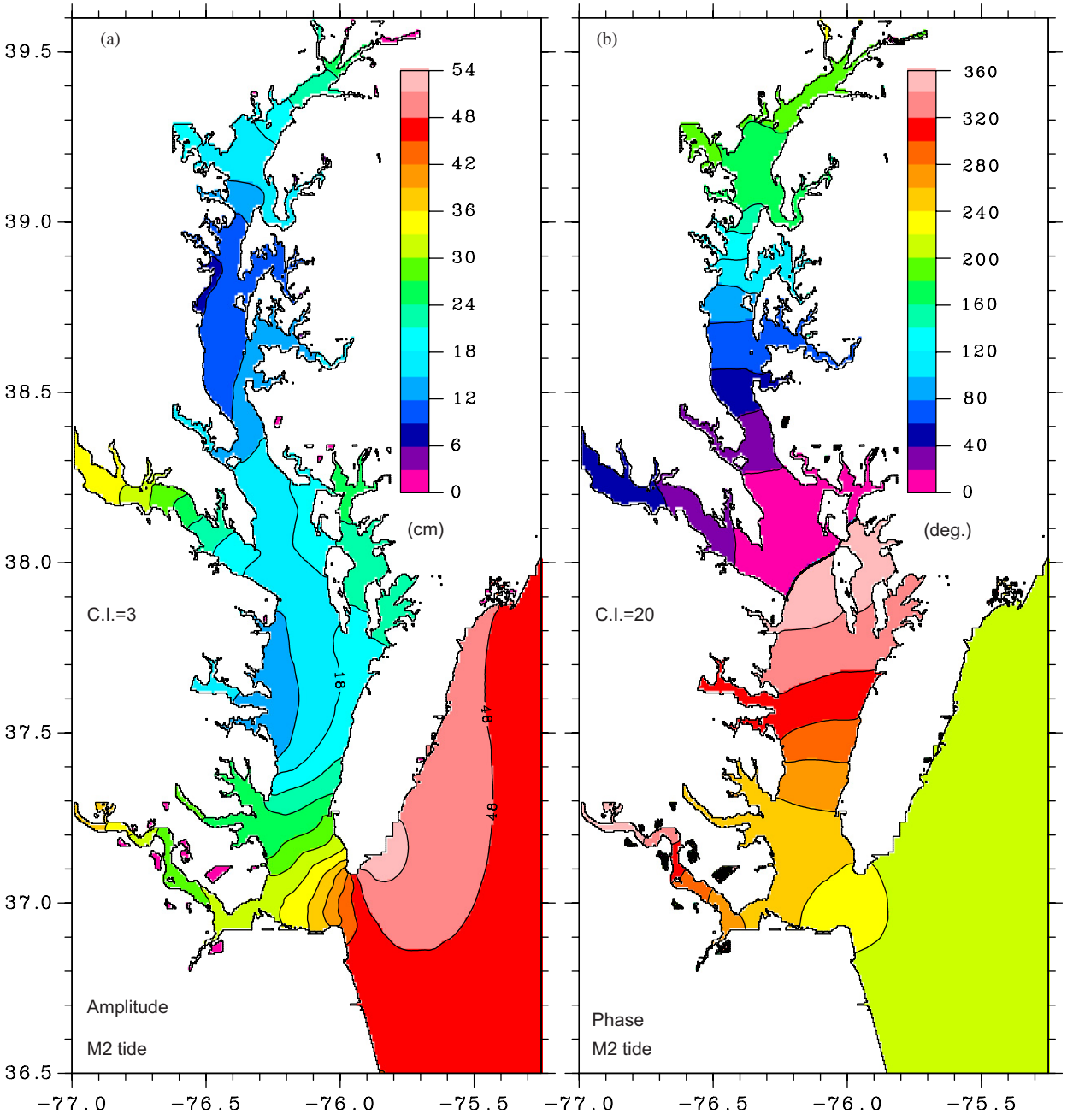

Fig. 2. Amplitude (a) and phase (b) of tide, calculated by Case 4.

3. Model results

3.1. Horizontal distribution of salinity and mean velocity

The mean velocity (thick line on Fig. 4a) and the mean barotropic velocity (thin line on Fig. 4a), which was calculated by averaging the corresponding velocity at all grids of the model domain, indicate that the motion reaches steady state at day ~200, although salinity continues to decrease (Fig. 4b). The baroclinic velocity, i.e., the difference between the two lines (mean and barotropic) for each case in Fig. 4a, evolves in the first 100 days and reaches an approximate steady state after day 200. Examination of the horizontal and vertical

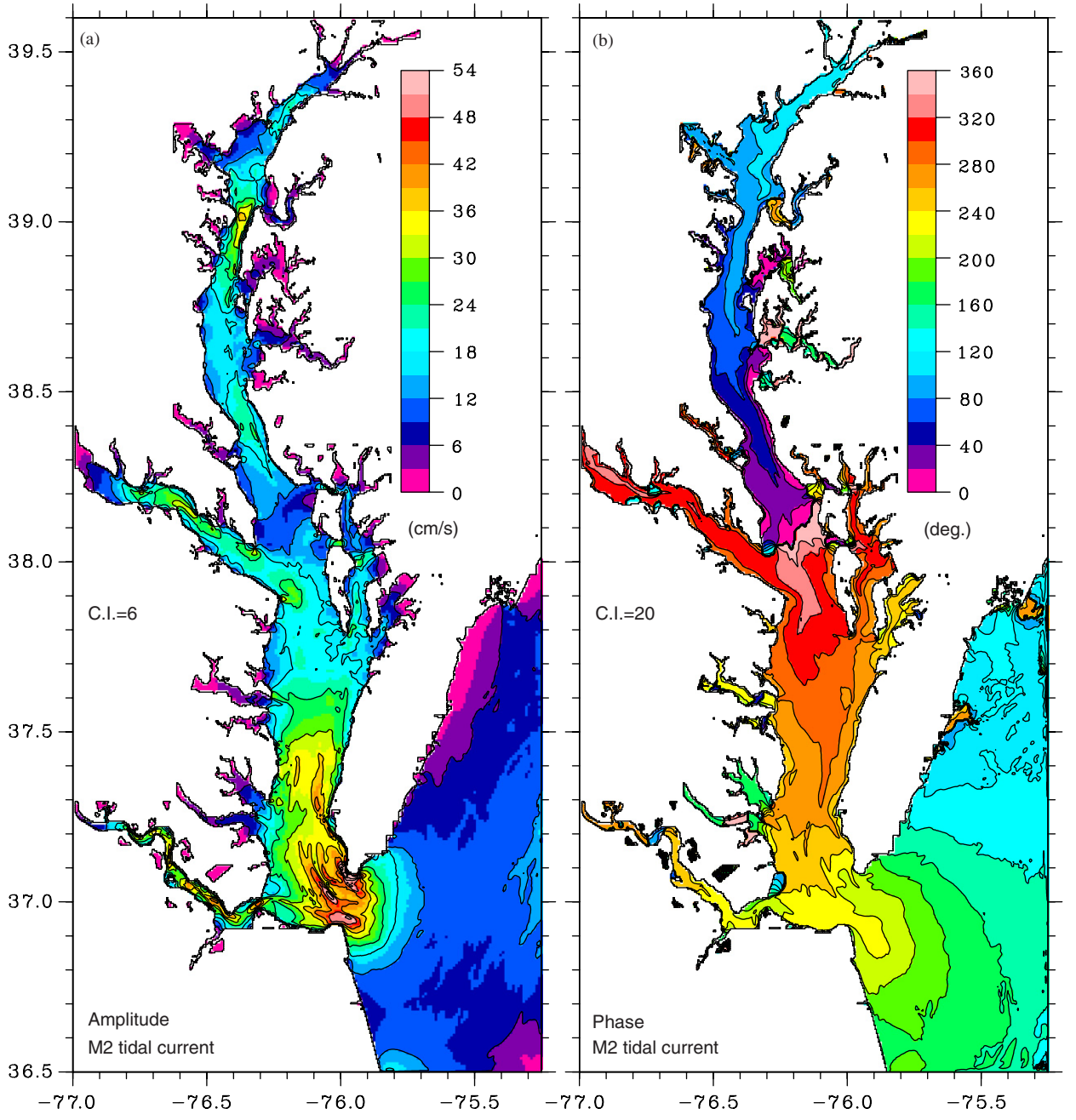

Fig. 3. Amplitude (a) and phase (b) of tidal current, calculated by Case 4.

distributions of velocity and salinity at different times (figures not shown here) shows that the velocity field in the entire domain and the salinity field outside the bay have small differences from day 180 to 240 to 300 to 360. The decrease in salinity portrayed in Fig. 4b occurs mostly inside the bay. The results of day 240 are chosen here as the solution to be examined in each case because the mean salinity inside the bay on day 240 is close to the observed value (~18 psu, Austin, 2002).

The general distribution of salinity inside the bay in the four cases (Figs. 5 and 6) is similar to observations (Pritchard, 1952). Observed features such as low salinity in the western side of the bay are consistent in the model results. The most significant differences in the salinity distributions among the

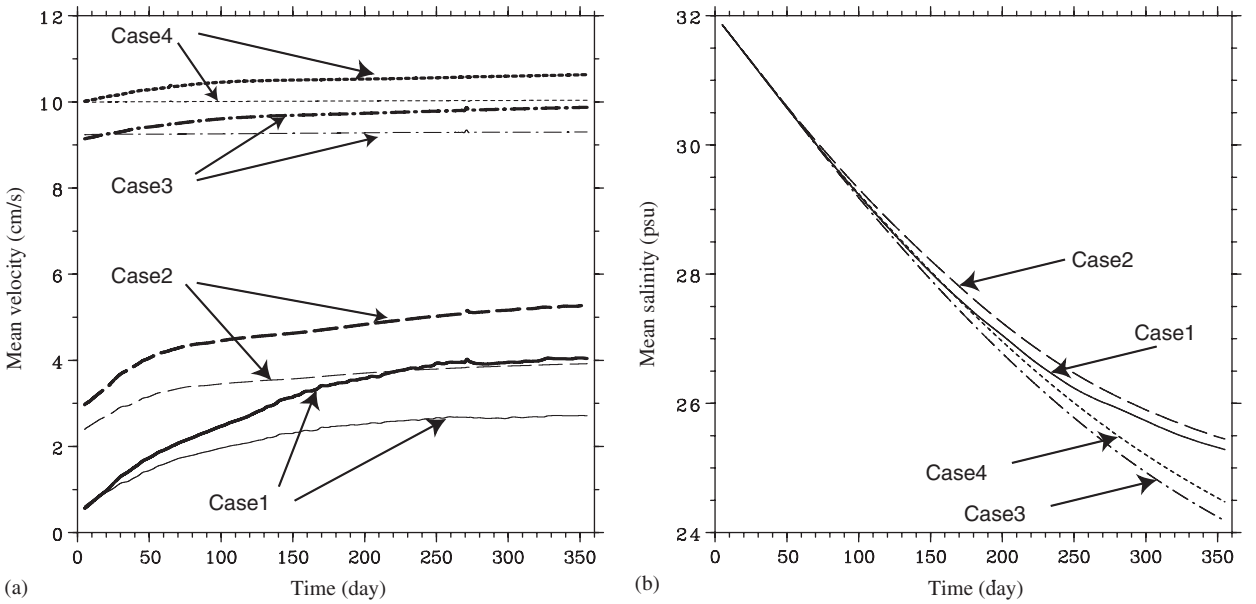

Fig. 4. Temporal variation of mean velocity (a) and mean salinity (b) in the entire model domain. The thin line in (a) is calculated by $1/N\sum_{i,j}(ua_{i,j}^2 + va_{i,j}^2)^{1/2}$, where ua and va are the vertically averaged velocity at grid point (i, j), N is the total number of grid points in the horizontal; the thick line is calculated by $1/N\sum_{i,j}1/M\sum_k(u_{i,j,k}^2 + v_{i,j,k}^2)^{1/2}$, where u and v are the velocity at grid point (i,j,k), M is the total number of grid points in the vertical.

four cases appear outside the bay. Case 1 produces a plume reaching 37.5 N, far upstream (in the sense of Kelvin wave propagation) from the mouth; the southward ambient coastal current in Case 2 largely corrects the northward plume but not completely; tidal forcing in Case 3 weakens greatly the northward plume; the combination of tidal forcing and ambient coastal current in Case 4 produces a plume similar to that observed by Marmorino et al. (2000).

A typical estuarine circulation with net seaward current in the upper layer and net landward current in the lower layer (not shown here) is obtained inside the bay in the four cases (Figs. 7 and 8). The inclusion of tide makes the current in the main stem of the bay to concentrate in the deep channel. The reason for this tidal effect on estuarine circulation is explained in Section 3.3. As with salinity, the most significant difference in the current fields is associated with the outflow plume outside the bay. The cases without tide produce a northward (upstream) branch of the outflow plume (Fig. 7), while the cases with tide produce an expected southward (downstream) plume (Fig. 8).

The influence of the ambient coastal current in modifying the northward plume is clear (Fig. 7), as suggested by previous plume simulations that a downstream ambient current can eliminate the upstream propagation of plume water on the shelf (e.g. Chapman and Lentz, 1994; Yankovsky and Chapman, 1997; Fong, 1998; Narayanan and Garvine, 2002). The tidal currents, however, also constrain the development of an upstream plume as shown in Fig. 8. A dynamical explanation on this phenomenon is given in Section 4.

3.2. Vertical structure of salinity and mean currents

An axial section along the bay displays a typical distribution of salinity and current in a partially mixed estuary (Fig. 9). The results of Cases 1 and 3 are not shown here because the ambient coastal current has little effects on the results inside the bay. Fig. 9a shows that salinity increases gradually from the head to the mouth of the bay and stratification is maintained in the vertical. The inclusion of tidal currents slightly decreases the salinity inside the bay and weakens the stratification (Fig. 9b). The salinity distribution shown in Fig. 9 is similar to observations in autumn and winter (Seitz, 1971). In spring and summer, however, the observed vertical stratification (Seitz, 1971) is stronger than the model results (Fig. 9). Surface heating and large fresh water discharge in spring and summer could cause the stronger stratification portrayed by the observations but remains to be explored further.

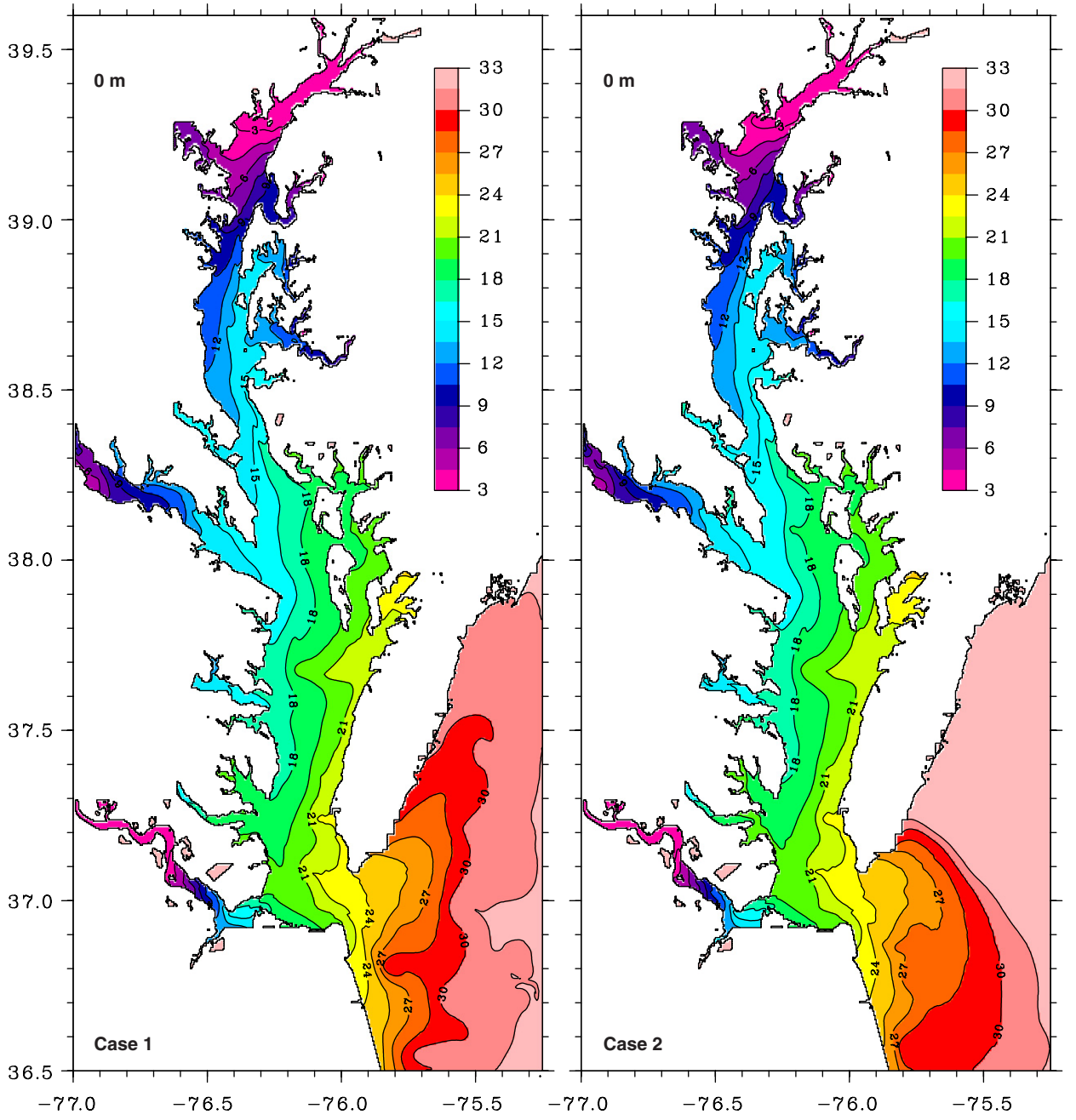

Fig. 5. Surface salinity simulated by the two cases without tidal forcing.

The mean currents along the longitudinal axis of the bay show a typical estuarine circulation with a seaward current in the upper layer and a landward current in the lower layer (Fig. 9c). The typical speed of the currents is 10–20 cm/s and the level of no motion is located roughly at 5 m. The inclusion of tidal forcing slightly weakens the landward current in the lower layer, deepens the level of no motion, and intensifies the seaward current in the upper layer (Fig. 9d). It must be noted that the intensified seaward current in the upper layer in Case 4 (Fig. 9d) is caused by the concentration of current in the central deep channel (Fig. 10). This concentration of mean outflow in the deep channel responds to the variation of vertical eddy viscosities and will be discussed in Section 3.3. In Fig. 10, the

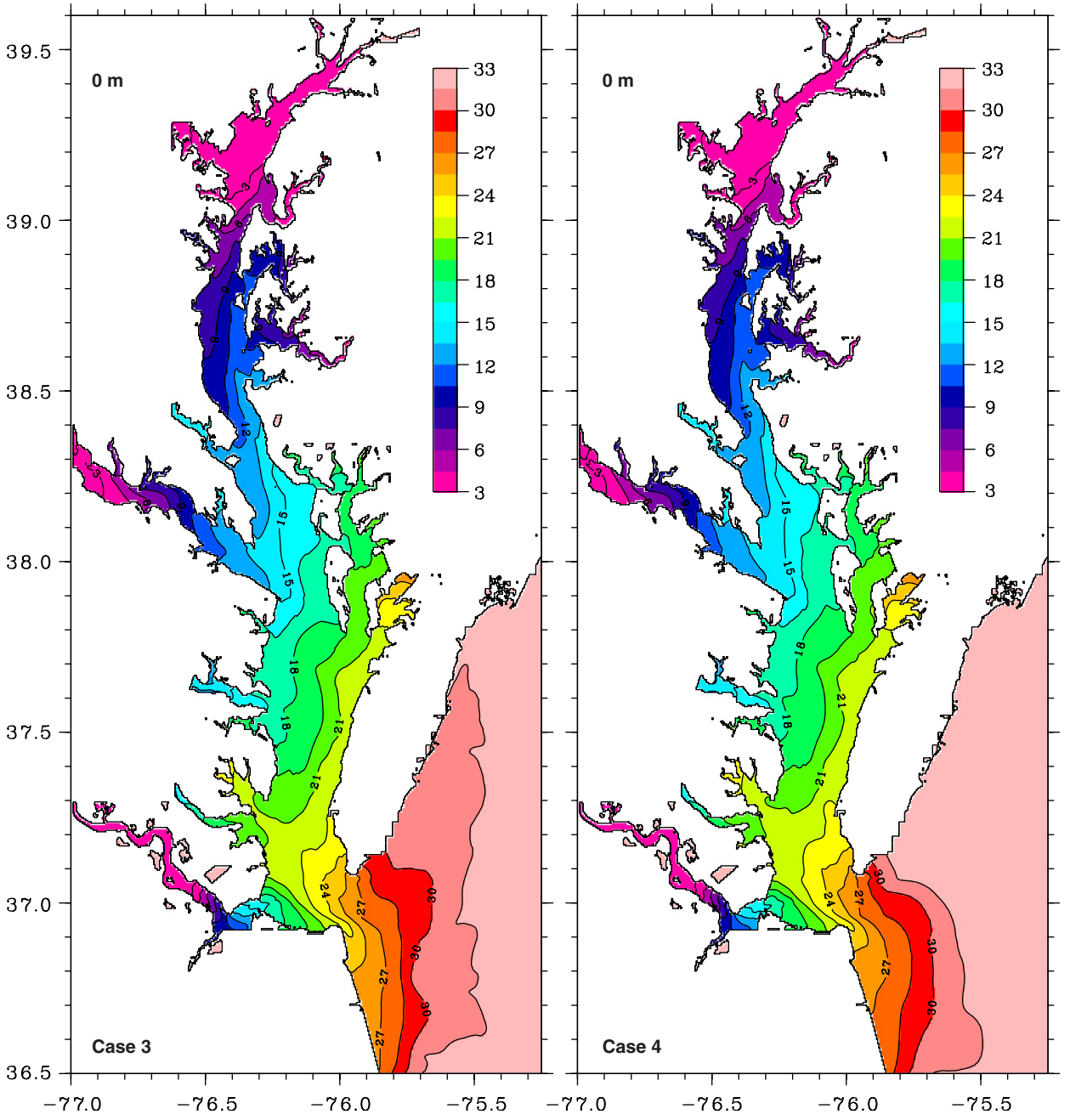

Fig. 6. Surface salinity simulated by the two cases with tidal forcing.

landward current is stronger in Case 2 than in Case 4, indicating that the tide weakens the landward current inside the Chesapeake Bay. The lifting of the level of no motion above the channel in Case 2 induces two cores of the seaward current in the surface layer. As the tide is included, the lifting of the level of no motion vanishes and the seaward current concentrates above the channel.

In order to further evaluate the vertical structure of the mean flow and salinity, a cross-section at the entrance (see Fig. 1 for its position) is chosen to correspond with that of observations by Valle-Levinson et al. (1998) and Reyes-Hernandez (2001). There are two channels in the section. The Chesapeake Channel is located in the southern side and the North Channel in the northern side. The shallow area

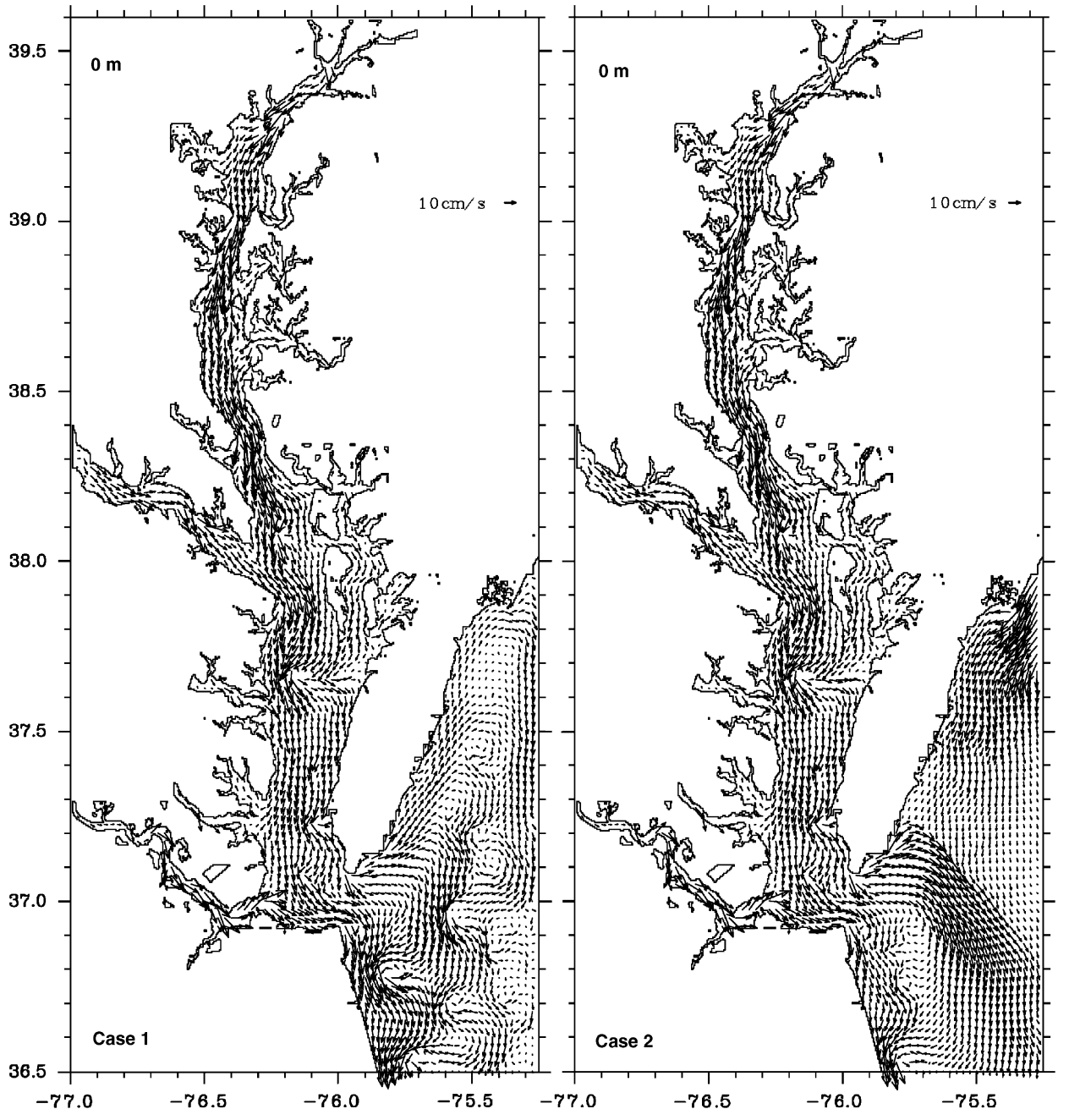

Fig. 7. Surface current simulated by the two cases without tidal forcing.

between these two channels is called Six-Meters Shoal. Model results show that salinity is lower in the southern than in the northern side of the bay entrance (Fig. 11a). Also, stratification is stronger in the Chesapeake Channel than in the North Channel. These features are consistent with observations (Valle-Levinson and Lwiza, 1997; Reyes-Hernandez, 2001) and are attributed to the competition between Earth's rotation and friction (Valle-Levinson et al., 2003). As tidal forcing is included, strong tidal currents around the entrance to the Chesapeake Bay (Fig. 3a) increase mixing and weaken stratification there (Fig. 11b), resulting in decreased vertical gradients but increased transverse gradients.

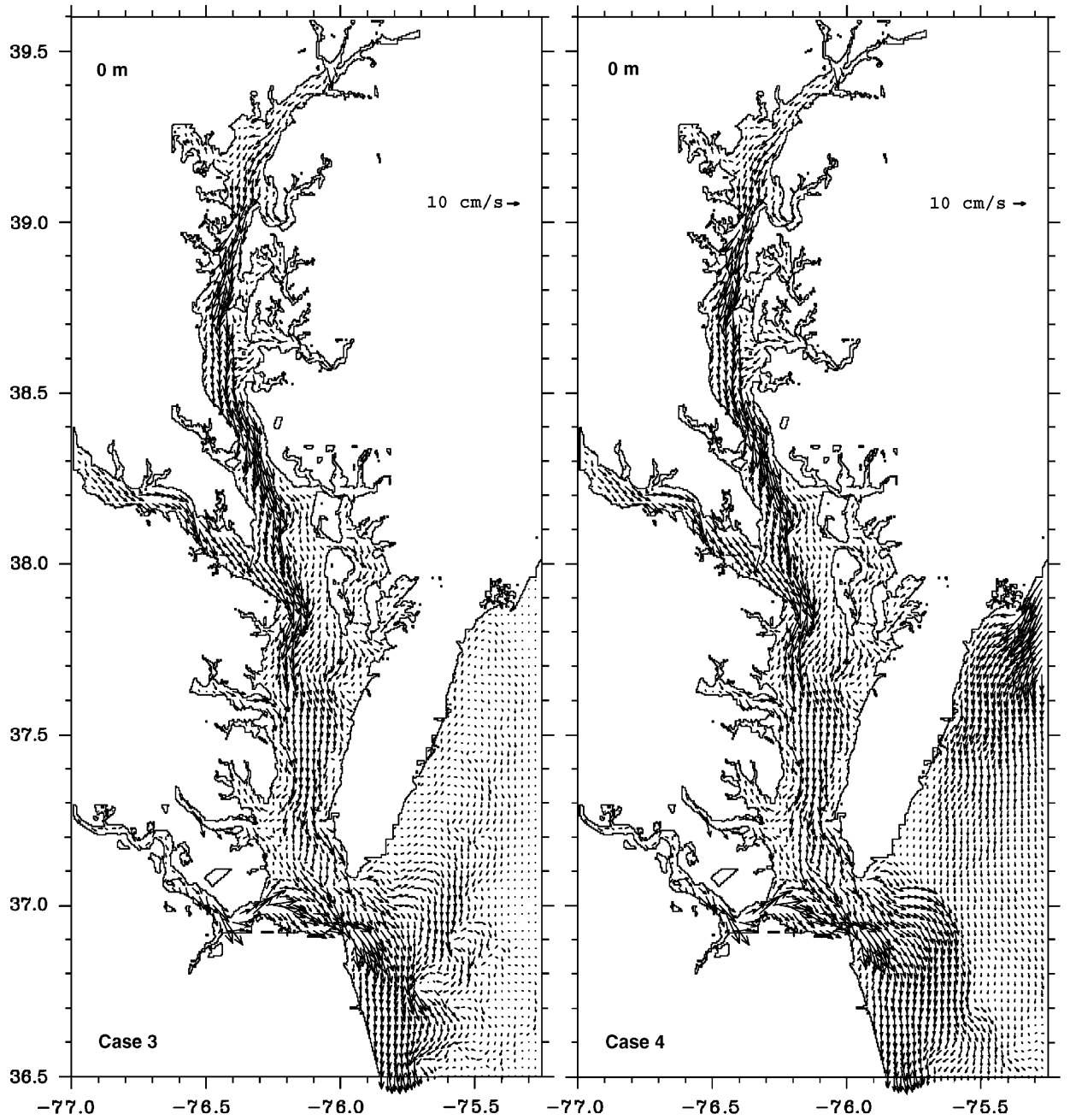

Fig. 8. Surface current simulated by the two cases with tidal forcing.

The vertical structure of the current across the section corresponds to a two-layered current in the main channel: outflow in the upper layer and inflow in the lower layer (Fig. 11c). Inflow appears only near the bottom of the two channels. The inclusion of tidal forcing transforms the level of no motion from being flat to being sloped (Fig. 11d). This indicates that tidal forcing produces larger horizontal gradients in the subtidal currents. Consequently, the outflow shifts to the southern part of the Chesapeake Channel and to the North Channel and a weak inflow appears between the two channels, i.e., over the Six-Meters Shoal. These distributions reproduced by the case with tide are

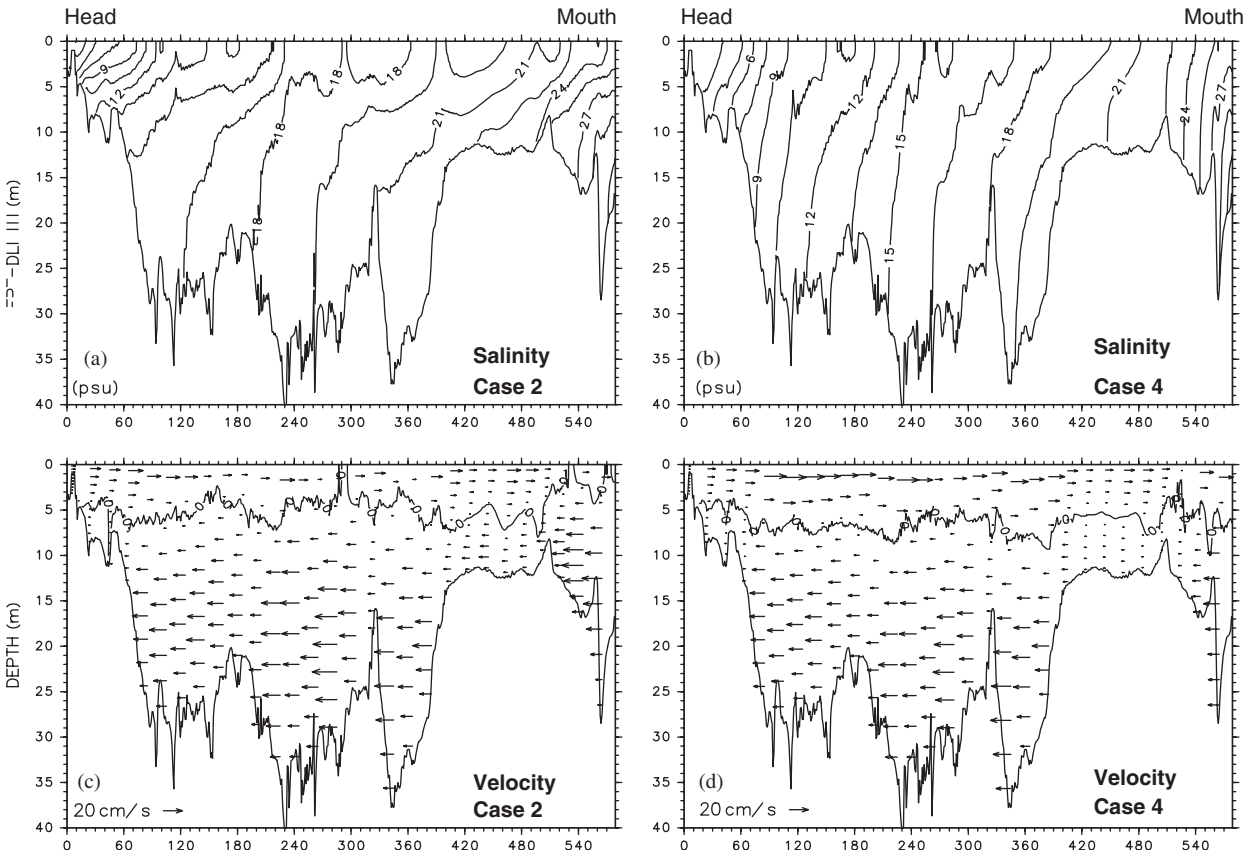

Fig. 9. Vertical distribution of salinity and mean current along the longitudinal axis of the bay (section A–A in Fig. 1), calculated by Cases 2 and 4. The unit of abscissa is grid number. The lines in (c) and (d) show the level of no motion.

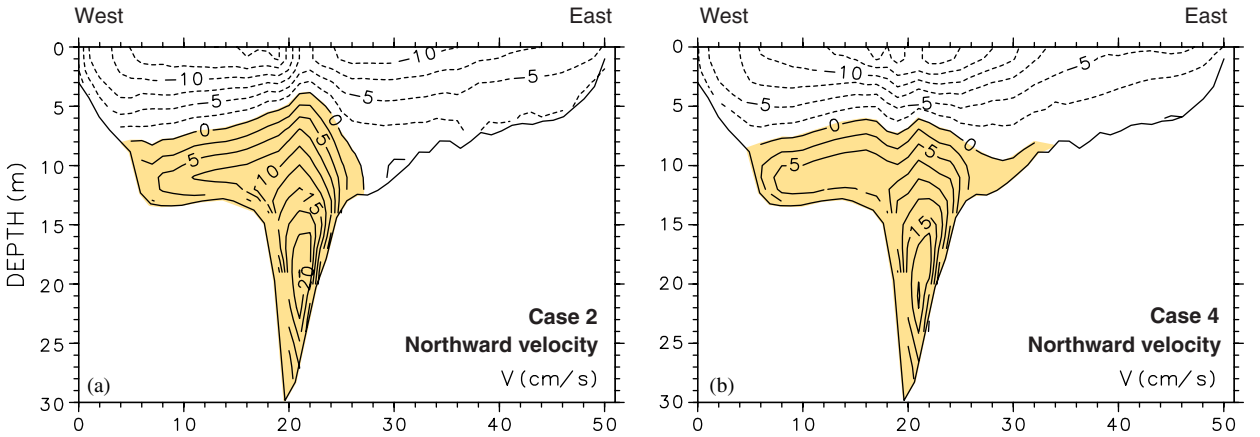

Fig. 10. Mean current across the section at 38.15 N in the middle bay (section B–B in Fig. 1). The unit of abscissa is grid number. Positive values denote northward current and negative values southward current.

remarkably similar to those observed by Valle-Levinson et al. (1998). In turn, the current along the section (transverse current) at the bay entrance is southward in the upper layer and northward in the lower layer (Fig. 11e). The strength of southward and northward currents is sensitive to

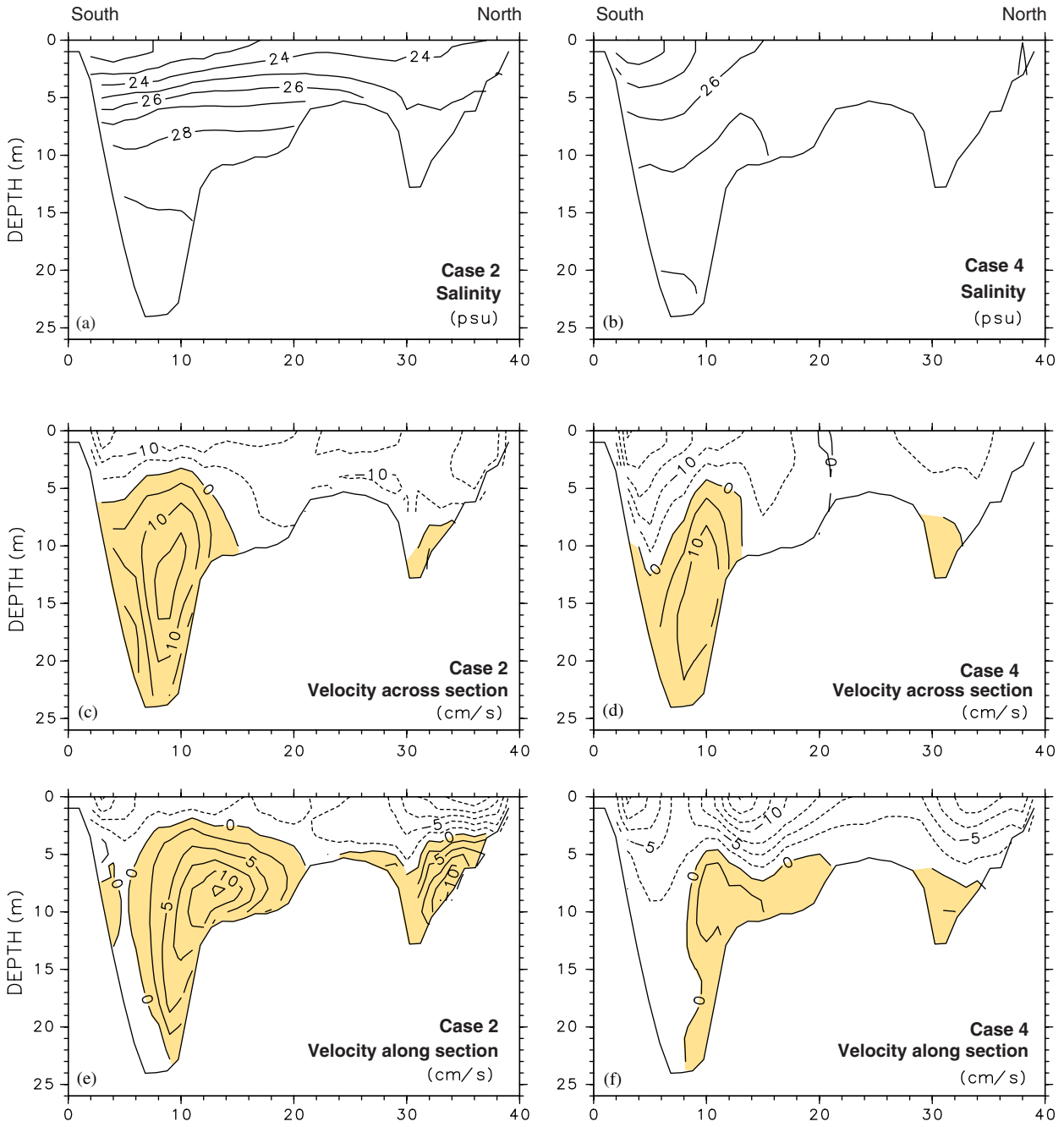

Fig. 11. Vertical distribution of salinity and the velocities across and along the section at the entrance of the bay (section C–C in Fig. 1). The unit of abscissa is grid number. Positive values in (c) and (d) denote inflow and negative values outflow. Positive values in (e) and (f) denote northward current and negative values southward current.

tidal forcing. In the case with tide, the northward current in the lower layer weakens largely and the southward current dominates the section (Fig. 11f).

In addition to river discharge and tidal forcing, wind forcing also influences the subtidal currents observed at the entrance. However, the essential features of the currents observed at the entrance to the Chesapeake Bay are that the outflow in the surface layer concentrates in the southern part of the Chesapeake Channel and in the North Channel. Also, the inflow concentrates in the lower layer of

the two channels. The level of no motion in Chesapeake Channel slopes steeply, and the current over the Six-Meters Shoal shows a weak inflow (Valle-Levinson et al., 1998). All these features are consistent with the results of Case 4 (Fig. 11d) rather than those of Case 2 (Fig. 11c). Furthermore, the observations show that the southward current in the surface layer dominates the current along the section at the entrance (Valle-Levinson et al., 1998). This is also consistent with the results of Case 4 (Fig. 11f) rather than those of Case 2 (Fig. 11e). Therefore, it can be concluded that tidal forcing is necessary to produce appropriate frictional influences that reliably represent the subtidal currents at the entrance to Chesapeake Bay.

3.3. Tidal effects on the vertical eddy viscosity

According to Kasai et al. (2000), friction plays a preponderant role in the transverse variability of exchange flows in estuaries. Valle-Levinson et al. (2003) use this finding to show that the spatial structure of exchange flows at the Chesapeake Bay entrance is explained by the influence of relatively large Ekman numbers (ratio of friction to Coriolis accelerations) with respect to a geostrophic exchange. The numerical results of Case 4 illustrate that the vertical eddy viscosity varies largely with inclusion of tidal forcing (Fig. 12). Compared to Case 2 (Fig. 12a), Case 4 shows that the vertical eddy viscosity increases significantly near the bottom throughout the bay and in the area near the entrance (Fig. 12b). Interestingly, at a transverse section in the middle of the bay (same as Fig. 10) the vertical eddy viscosity decreases slightly from Case 2 (Fig. 12c) to Case 4 (Fig. 12d) near the interface between seaward and landward currents. This might result from decreased vertical shears in Case 4 relative to Case 2. At the transverse section in the bay entrance, the vertical eddy viscosity increases significantly in the entire section from Case 2 (Fig. 12e) to Case 4 (Fig. 12f).

The weakening of landward flows in Case 4 relative to Case 2 (Figs. 9 and 10) is a natural response to the increase of vertical eddy viscosity near the bottom from the inclusion of tidal forcing. The transverse structure of exchange flows in the middle bay (Fig. 10) and at the entrance (Fig. 11) is consistent with the analytical solution given by Valle-Levinson et al. (2003). The numerical results were consistent with the analytical in the sense that inflows and outflows are concentrated in the channel under relatively weak friction but segregate horizontally as friction increases. In the middle bay, the apparent larger viscosity in Case 2 lifts the interface of exchange flows upward, i.e., causes the core of net outflow to shift away from the channel (Fig. 10a). In Case 4, reduced viscosity (friction) allows the net outflow core to appear in the channel (e.g. Valle-Levinson et al., 2003). At the bay entrance, larger friction in Case 4 increases the tilt of the interface between inflows and outflows (Fig. 11d). This causes weaker net outflows over the deepest part of the section than in Case 2 and also induces larger horizontal variations of exchange flows.

4. The plume outside the bay

As shown in Figs. 6 and 7, Case 1 produces a northward plume outside the Chesapeake Bay. The ambient coastal current in Case 2 largely corrects the northward plume but not completely. Tidal forcing in Case 3 weakens the northward plume but cannot eliminate it. The combination of ambient coastal current and tidal forcing in Case 4 produces a realistic plume outside the Chesapeake Bay. If we follow the plume classification of Yankovsky and Chapman (1997), Case 1 seems to represent an extreme case of surface-advected plume and Case 4 illustrates a bottom-advected plume. These concepts are explained next.

4.1. Surface-advected plume versus bottom-advected plume

On the basis of the vertical structure of a plume, Yankovsky and Chapman (1997) suggested two extreme cases of river plumes: a bottom-advected plume and a surface-advected plume (see Figs. 1 and 2 of Yankovsky and Chapman, 1997). In the bottom-advected plume, the plume water occupies the entire water column and turns right immediately after it flows out of the estuary mouth. The outflow associated with the bottom-advected plume is in contact with the bottom. In the surface-advected plume, the plume water stays on the surface layer forming a thin layer above the ambient denser water. The plume typically forms a bulge near the estuary mouth within which an anticyclonic flow is generated. The outflow associated with the surface-advected plume is limited to the surface layer and essentially remains detached from the bottom.

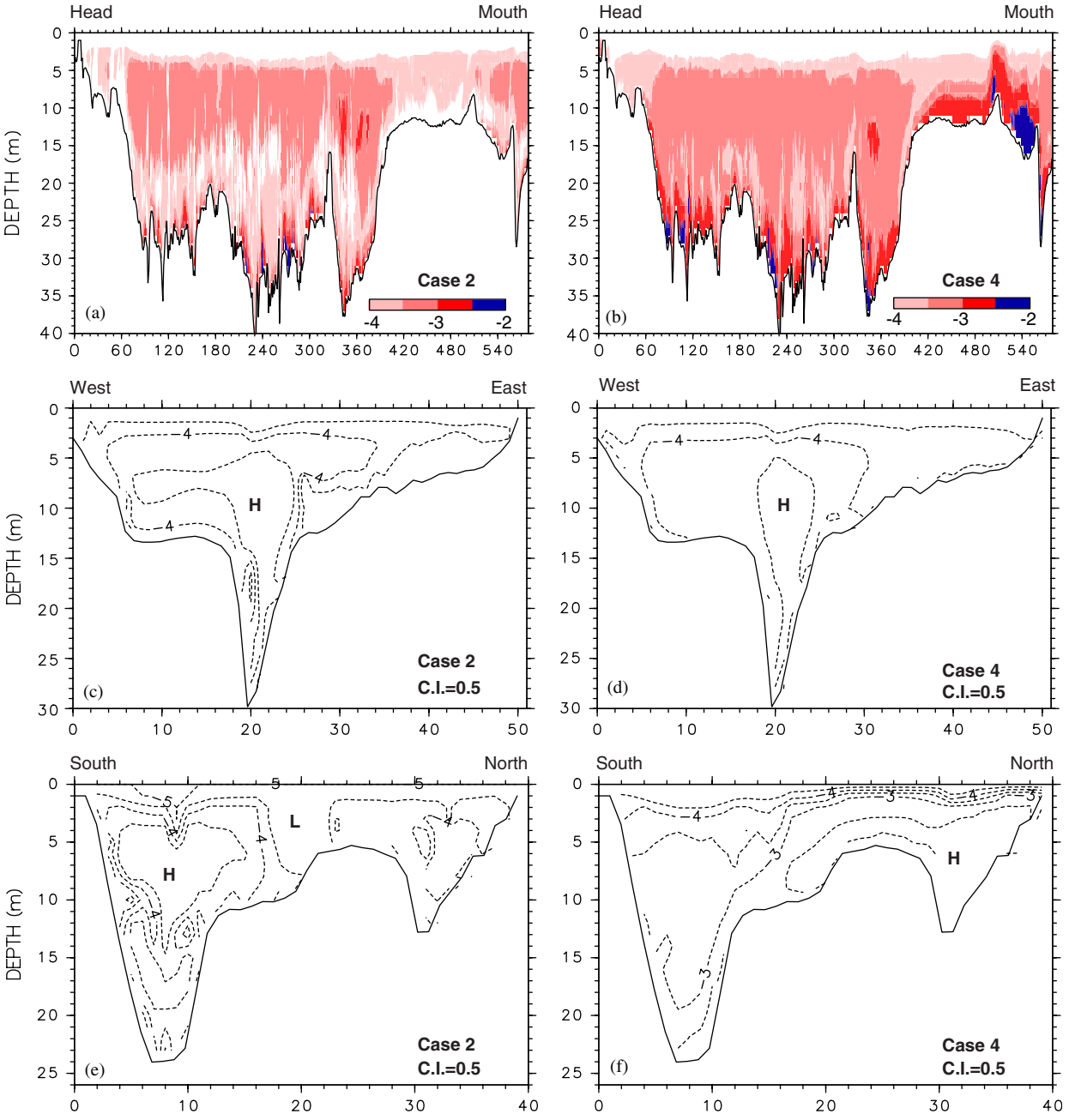

Fig. 12. Vertical eddy viscosity coefficients along the section of longitudinal axis of the bay (section A–A in Fig. 1), along the section at 38.15 N in the middle bay (section B–B in Fig. 1), along the section at the entrance of the bay (section C–C in Fig. 1). The unit of abscissa is grid number. Values are base-10 logarithmic scale of vertical eddy viscosity coefficients (m^2/s).

The northward plume outside the Chesapeake Bay produced by Case 1 resembles the well-known upstream intrusion of buoyant water from an inlet into the shelf (Garvine, 2001). Garvine (2001) noted that the upstream intrusion of buoyant water is often found in the results of numerical models (Chapman and Lentz, 1994; McCreary et al., 1997; Fong, 1998; Garvine, 1999, 2001; Yankovsky, 2000; Narayanan and Garvine, 2002), but it is rarely observed in the real ocean. In addition to the upstream intrusion of buoyant water, numerical models also tend to produce a type of plume with a

massive anticyclonic bulge near the mouth of estuary (Pichevin and Nof, 1997; Nof and Pichevin, 2001; Garvine, 2001; Nof, 2005), which is also rarely observed in the real ocean (Garvine, 2001). Moreover, these two types of plumes do not reach a steady state, even for steady forcing (Pichevin and Nof, 1997; Garvine, 2001; Nof, 2005).

Garvine (2001) suggests that the unrealistic aspects in model configuration such as a simple inlet, a deep coastal wall or a large angle (usually 90°) between the inlet channel and coastal wall of shelf are the fundamental causes for producing the upstream intrusion. Yankovsky(2000) pointed out that the oversimplification of the boundary conditions, such as uniform velocity in the vertical applied for buoyant discharge at the mouth, blocks the landward flow in the lower layer and initiates the upstream spreading of buoyant flow. In our model configuration, the buoyant discharge enters the shelf through a natural mouth where the landward current in the lower layer is not blocked. The only concern is the coastal wall. Because of the inclusion of tidal forcing, we set the minimum water depth in the model as 3 m that is larger than the 0.1 m used by Garvine (2001) in an experiment showing effects of a coastal wall on the upstream intrusion of buoyant water.

The inclusion of an ambient current flowing in the downstream direction has been shown to restrain the upstream intrusion of buoyant water (Chapman and Lentz, 1994; Yankovsky and Chapman, 1997; Fong, 1998; Narayanan and Garvine, 2002). Garvine (2001) noted that this method is not a universal remedy for models reproducing a realistic plume. With no downstream flowing ambient current, but improving the model configuration with shallow depths (0.1 m) at the coast, Garvine (2001) showed that the upstream intrusion of buoyant water almost disappears. However, the improvement of model configuration is usually limited in a realistic application. For example, simulations in Chesapeake Bay with tidal forcing hinder the use of a coastal wall 0.1 m deep as used by Garvine (2001) because of numerical stability problems.

Therefore, a downstream ambient current was also added in Case 2 to correct the northward intrusion appearing in Case 1. On the other hand, as noted in Section 2, observations also support a southward ambient current outside the Chesapeake Bay (Beardsley and Boicourt, 1981; Epifanio and Garvine, 2001). As shown in Figs. 5 and 7, the downstream ambient current largely corrects the northward plume but not completely. This can be understood as follows. In the simulation, the reproduced current structure at the bay entrance acts as a boundary condition to the plume outside Chesapeake Bay. The current structure at the bay entrance without tide is favorable to form an upstream intrusion of buoyant water along the shelf in Case 1. Although the ambient current can restrain the northward plume by advecting the buoyant water southward, it cannot eliminate the drive of the northward plume. This is because the ambient coastal current has a minor, apparently negligible, effect on the subtidal circulation inside Chesapeake Bay.

As shown later, the inclusion of tidal current is a necessary condition to produce a correct plume structure at the mouth, which in turn affects the upstream intrusion of buoyant water in the shelf. Chao (1990) emphasized the effects of tide-induced residual eddies on the plume in a coupled plume–shelf system but did not mention the change of vertical structure of the subtidal current at the estuary mouth. (The cyclic condition used in his model configuration is questionable because the buoyancy-driven coastal current is stronger in the downstream area than in the upstream area and a cyclic condition implicitly imposes an unrealistic downstream ambient current in the shelf.) Garvine (1999) examined the tidal effects on the downstream penetration of buoyant water and concluded that shelf tides have a detectable but moderate influence on plume downstream penetration. In the same paper, he also mentioned that the upstream penetration is reduced with tides but did not analyze its details. Garvine (2001) showed that a sinusoidally varying alongshelf wind can reduce the upstream penetration speed from 2.08 to 1.54 cm/s and mentioned that the effects of shelf tides are similar with a varying wind but did not present the results with shelf tides. By introducing a variable discharge at the estuary mouth at tidal frequencies, Yankovsky et al. (2001) concluded that tidal fluctuations in the inflow of buoyant discharge has minor effects on the buoyant plume along the shelf. Recently, Isobe (2005) demonstrated that the alongshore component of tidal currents effectively stabilizes the offshore growth of a river-plume bulge.

In addition to the above explicit results on the tidal effects on the plume, Yankovsky (2000) and Garvine (2001) also studied the effects of vertical viscosity and vertical mixing on the upstream intrusion of buoyant water. In particular, Garvine

(2001) presented an analytic solution to demonstrate that reduced vertical mixing and increased vertical viscosity tend to reduce the upstream intrusion speed. Because tidal currents tend to simultaneously increase vertical mixing and vertical viscosity, the tidal effects on the upstream intrusion of the plume are not easily interpreted from the analytic solution given by Garvine (2001).

In a coupled estuary–shelf system, tidal effects on the plume outside the estuary include two aspects. The first is the direct effect on the buoyancy-driven coastal current. This issue has been studied by the use of an artificial estuary mouth and shelf domain (Garvine, 1999, 2001; Yankovsky, 2000). The other aspect is the influence of tidal currents on the subtidal current structure inside the estuary and in turn the outflow at the mouth of estuary. This aspect is identical to how the tide affects the boundary condition given at the artificial estuary mouth in the simulation with only shelf domain (Garvine, 1999, 2001; Yankovsky, 2000). Since this issue has not been fully addressed in the previous studies, Case 1 through 4 are interpreted in terms of the vertical structure of the plume for each case.

In the cases without tide (Fig. 5), the plume is similar to a surface-advected plume, while in the cases with tide (Fig. 6) the plume emulates a bottom-advected plume. Obviously, the tide makes the river plume shift from a surface-advected plume to a bottom-advected plume and this change should relate to the variation in the vertical structure of plume. The vertical distribution of salinity along a section that crosses the plume outside the bay confirms this inference (Fig. 13). In the cases without tide (Figs. 13a and b), the isohalines lean toward the plume front (Fig. 13a), similarly to the surface-advected plume shown by Yankovsky and Chapman (1997). The inclusion of ambient coastal current cannot change this basic structure (Fig. 13b). In the cases with tide (Figs. 13c and d), the salinity becomes vertically well mixed and this vertical structure is consistent with the isohalines

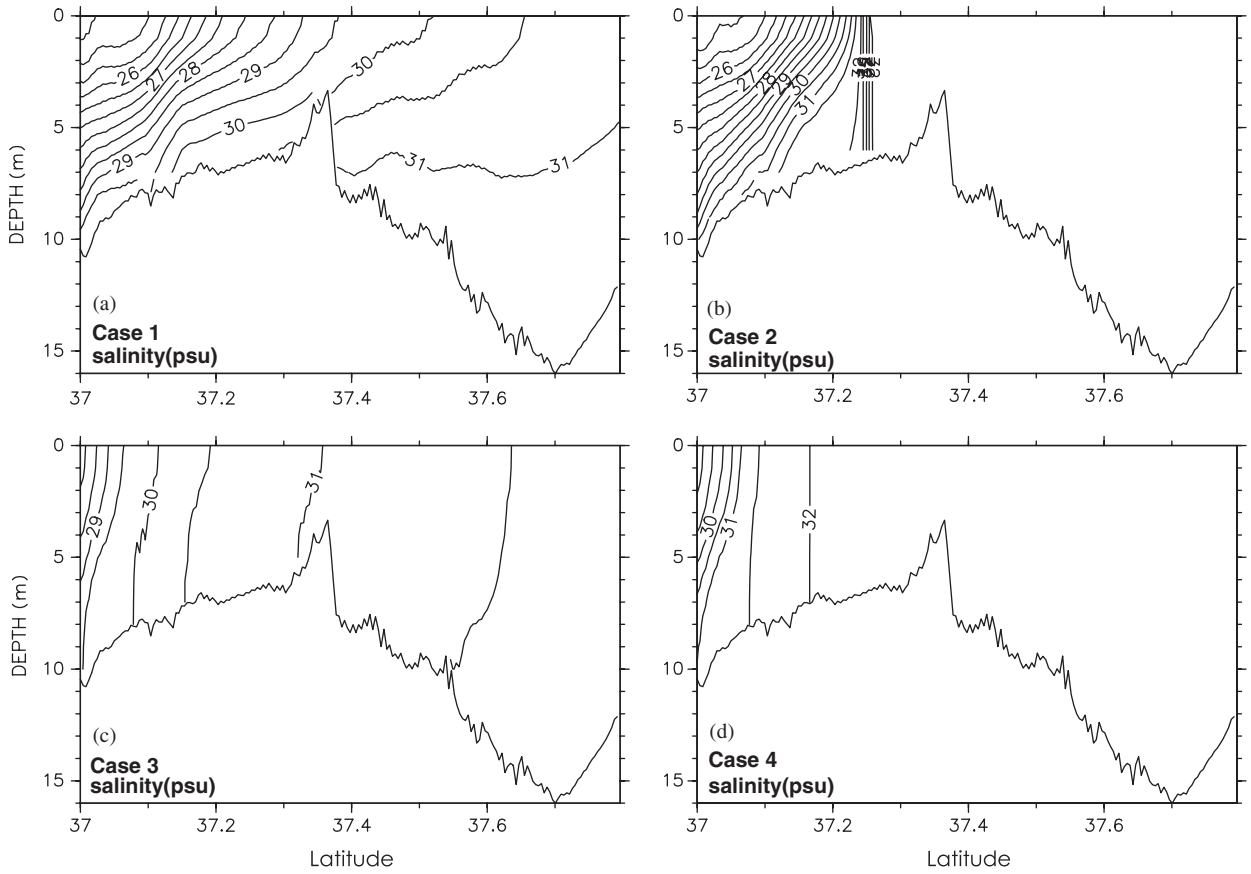

Fig. 13. Vertical distribution of salinity in four cases along the section across the plume outside the bay (section D–D in Fig. 1).

structure of the bottom-advected plume shown by Yankovsky and Chapman (1997). Returning to the vertical distribution of exchange flows at the bay entrance (Fig. 11), the outflow in the region <8 km is more in contact with the bottom in Case 4 than in Case 2. This again confirms the inference that tidal forcing transforms the outflow of Chesapeake Bay water from a surface-advected plume to a bottom-advected plume by altering the vertical structure of outflow of buoyant discharge. Because the tidal current has a spring–neap cycle and the fresh water discharge also changes temporally, the bay plume can also behave as a surface-advected plume, especially when high fresh water outflow occurs in a neap tide period.

Garvine (1999) showed that the simulated plume is sensitive to the background eddy viscosity or diffusivity in the Mellor–Yamada turbulent closure model used to avoid zero viscosity or diffusivity when the local Richardson number exceeds about 0.2. However, the results presented here are not as sensitive to the background viscosity as Garvine's results. Fig. 12 indicates that the vertical eddy viscosity given by the turbulence model is larger than the background value used, in particular in the case with tide.

Chapman and Lentz (1994) explain the upstream movement of a plume along the shelf as a self-advected process. Applying their explanation to the northward movement of the plume outside the bay, a positive acceleration of northward velocity and a negative temporal variation of salinity are necessary near the plume front. To confirm these two points, the terms in the momentum equation are analyzed for the northward velocity and the terms in the conservation equation for salinity are evaluated.

4.2. Dynamics of northward velocity

The momentum equation for the northward velocity v can be expressed as

$$\frac{\partial v}{\partial t} + ADV = PRE + COR + VDIF, \tag{3}$$

where ADV denotes advection terms, PRE denotes pressure gradient, COR denotes Coriolis force, $VDIF$ denotes the internal stress divergence related to vertical eddy viscosity. The stresses related to the horizontal viscosity are small enough to be negligible. All these terms are calculated by POM and the tidal components are removed with a tide killer filter (Hanawa and Mitsudera, 1985).

In Figs. 14 and 15, surface distributions of each term in Eq. (3) are presented for all of the four cases, plus the isohaline of 31.5, which approximately represents the plume front (Fig. 13). The dynamics terms are shown on day 100 and the salinity contours on days 90, 120, and 150. The plume front in Case 1 moves northward with a speed of 0.7 km/day ($\sim$0.8 cm/s). Behind the plume front, i.e., south of the plume front, there is an area with positive acceleration close to the coast (Fig. 14a). The plume front in Case 3 also moves northward. Its speed is smaller than that in Case 1. The positive acceleration of northward velocity behind the plume is weaker in Case 3 than in Case 1. In Cases 2 and 4, positive acceleration of northward velocity behind the plume weakens greatly because of the ambient flow and tidal forcing (Figs. 14b and d).

The advection terms (Figs. 14e–h) are generally small except for the bay entrance in the cases with tide and the northeastern corner where the ambient coastal current is imposed. In the cases with tide, tidally averaged advection terms correspond to the generation of tide-induced residual current, which is appreciable around the entrance to the bay.

The combination of pressure gradient and Coriolis force (Figs. 14i–l) is responsible for the positive acceleration of northward velocity behind the plume front. This is particularly clear in Case 1 (Fig. 14i). Fig. 15 indicates that the positive acceleration of northward velocity is caused by the pressure gradient. In Case 1 (Fig. 15e), an area with positive pressure gradient exists from the bay entrance to the plume. The ambient coastal current in Case 2 brings negative pressure gradient ahead of the plume front, i.e., north of the plume front. Tidal forcing in Case 3 weakens the positive pressure gradient behind the plume front.

Internal stresses (Figs. 15a–d) vary greatly with the inclusion of tidal forcing. Behind the plume front, internal stresses show negative values and therefore act to prevent the northward movement of the plume. In Case 1 (Fig. 15a), negative internal stresses are very weak and allow northward propagation. In Case 3 (Fig. 15c), stresses increase greatly. Therefore, tidal forcing increases internal stresses in the plume front area and hinders northward plume propagation.

Further analysis may be derived from the salinity equation, which can be expressed as

$$\frac{\partial S}{\partial t} + ADVS = VDIFS, \tag{4}$$

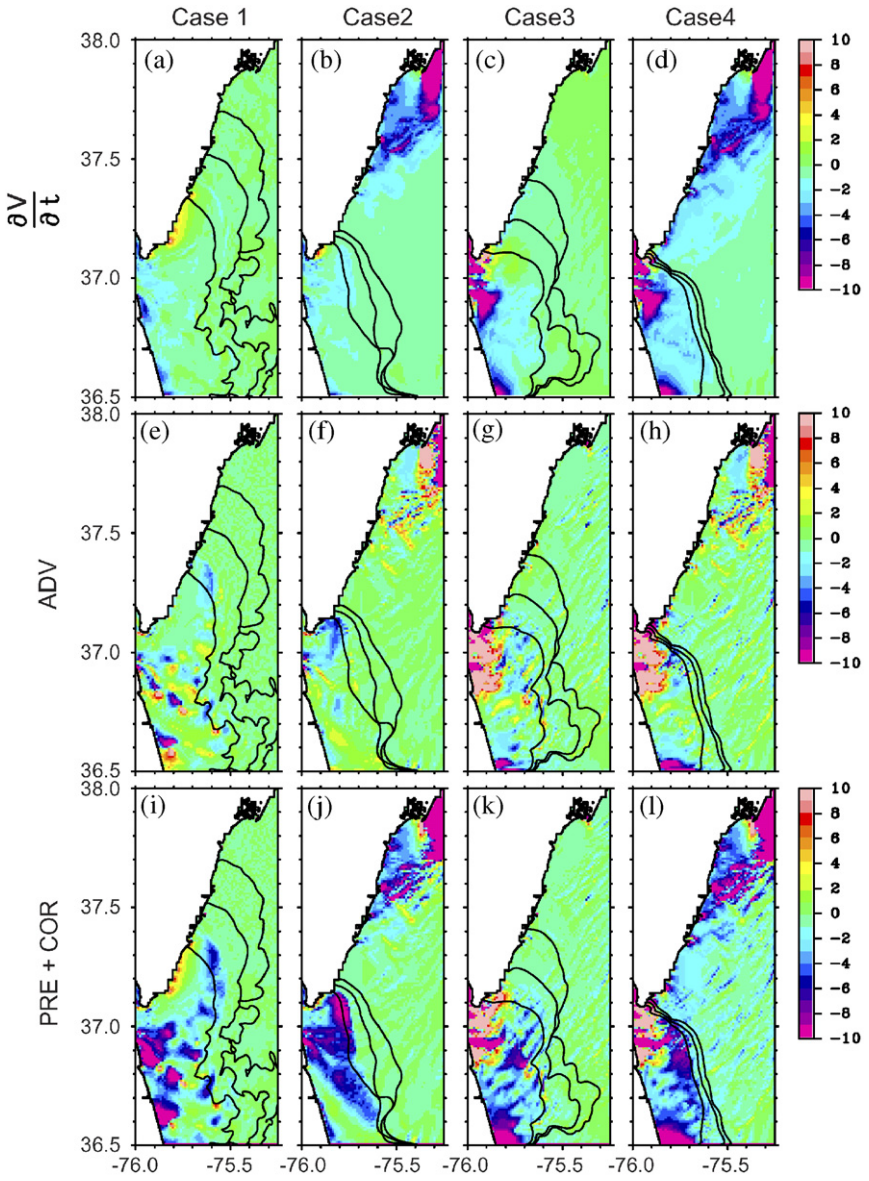

Fig. 14. Local acceleration (top panels), advection (middle panels), and combination of pressure gradient and Coriolis force (bottom panels) in the momentum equation for northward velocity at surface layer on day 100. The contours show the position of 31.5 psu on days 90, 120, and 150 that moves northward. The values of $\partial v/\partial t$, ADV, and $PRE+COR$ have been multiplied by a factor of $24 \times 3600 \times 50$.

where S denotes salinity, $ADVS$ denotes advection, and $VDIFS$ denotes vertical diffusivity. Similarly to the momentum Eq. (3), horizontal diffusivity is negligible.

The temporal variation of salinity around the plume front is negative in all the four cases (Fig. 16), indicating a decrease of salinity. The magnitude of the negative temporal variation of salinity around the plume front in Cases 1 and 2 is large while that in Cases 3 and 4 is small. Fig. 16 indicates that the imbalance between advection and vertical diffusivity causes the decrease of salinity.

The advection of salinity in Fig. 16 is then separated into two components: horizontal and vertical (Fig. 17). Around the plume front, horizontal advection is positive and vertical advection is negative. This suggests that vertical advection compensates the salinity loss caused by horizontal advection. In Cases 1 and 2, horizontal advection is not balanced by vertical advection. However, in

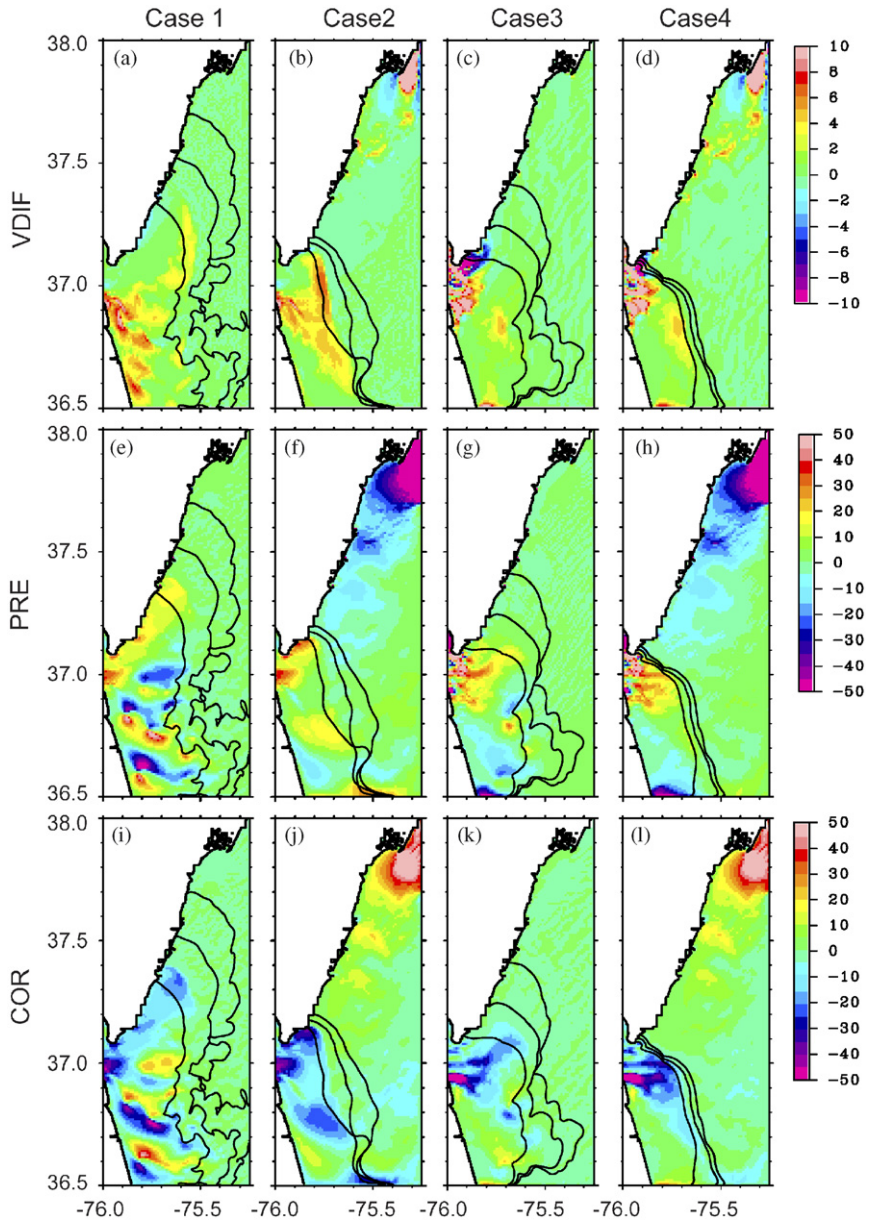

Fig. 15. Vertical viscosity (top panels), pressure gradient (middle panels), and Coriolis force (bottom panels) in the momentum equation for northward velocity at surface layer on day 100. The contours show the position of 31.5 psu on days 90, 120, and 150 that moves northward. The values of *VDIF*, *PRE*, and *COR* have been multiplied by a factor of $24 \times 3600 \times 50$.

Cases 3 and 4, advection in the two directions is nearly balanced. Therefore, the self-advected process of an upstream intrusion of a plume along the shelf, as suggested by Chapman and Lentz (1994), is confirmed in the cases without tide. In Case 1, the northward pressure gradient behind the plume front is not balanced by the other terms and produces a positive acceleration of northward velocity along the coast north of the entrance. Meanwhile, horizontal advection of salinity is not balanced by the other processes and causes the decrease of salinity. These two effects make the plume propagate northward. On the other hand, the inclusion of tidal forcing increases friction, decreases the northward pressure gradient around the plume, and makes the horizontal and vertical advection of salinity to be balanced.

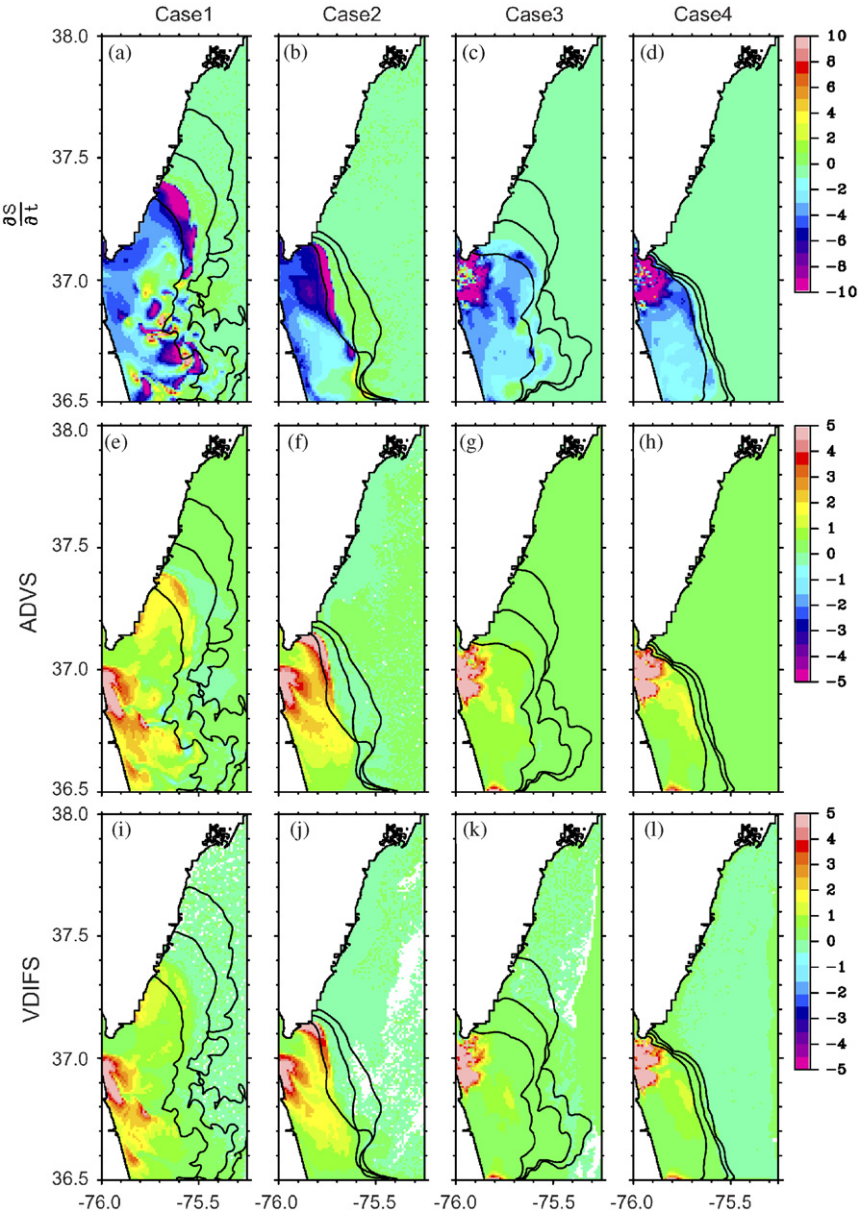

Fig. 16. Temporal variation (top panels), advection (middle panels), and vertical diffusion (bottom panels) in the salinity equation at the surface layer on day 100. The contours show the position of 31.5 psu on days 90, 120, and 150 that moves northward. The values of $\partial S/\partial t$ have been multiplied by a factor of $24 \times 3600 \times 10$, those of *ADVS* and *VDIFS* by a factor of $24 \times 3600 \times 100$.

Therefore, the northward plume outside the bay is severely hampered by these processes.

5. Conclusions

Tidal forcing affects not only estuarine circulation and the salinity distribution inside the Chesapeake Bay but also the river plume outside the bay. Increased mixing by tidal currents weakens stratification. Inside the bay, the seaward flow in the surface layer concentrates in the deep channel and the landward flow in the bottom layer weakens. Additionally, tidal forcing induces large horizontal variation of exchange flows at the bay entrance and makes the outflow plume to be in contact with the bottom. Consequently, a bottom-advected plume is formed in the presence of tidal forcing. Within the plume outside the bay, tidal currents increase

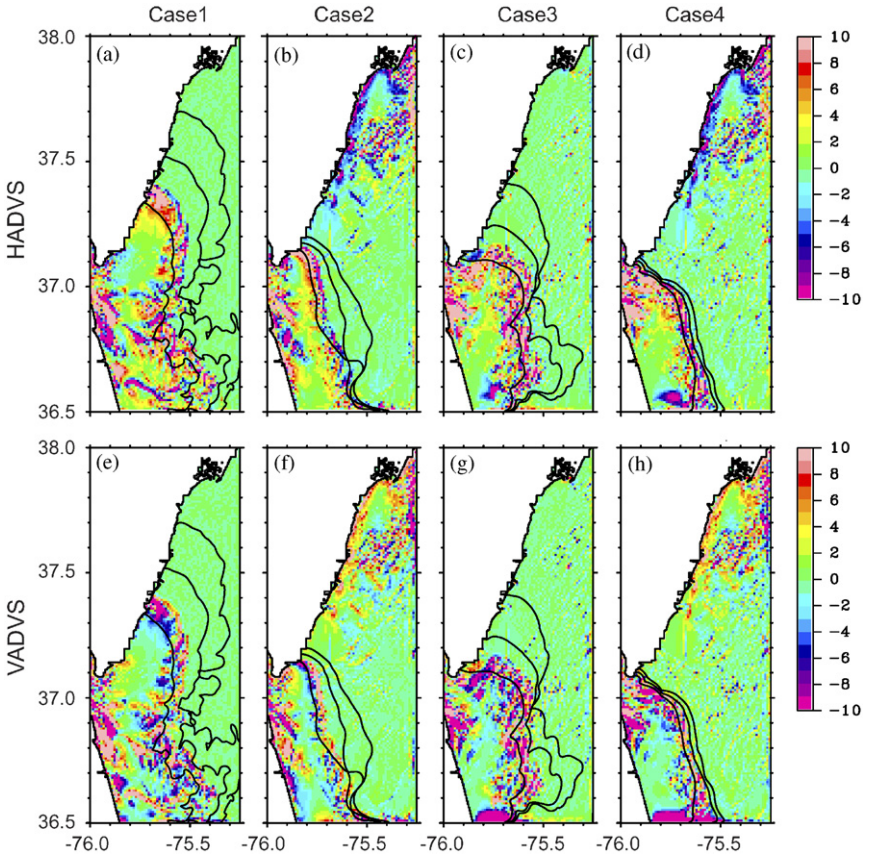

Fig. 17. Horizontal advection (top panels) and vertical advection (bottom panels) in the salinity equation at the surface layer on day 100. The contours show the position of 31.5 psu on days 90, 120, and 150 that moves northward. The values of *HADVS* and *VADVS* have been multiplied by a factor of $24 \times 3600 \times 10$.

friction, and make horizontal and vertical advection of salinity to be balanced. These two effects, favored by tidal forcing, hinder the upstream movement of the plume. In general, because the transverse structure of exchange flows in estuaries is sensitive to friction (Valle-Levinson et al., 2003), which is greatly affected by tidal forcing, inclusion of tidal forcing is necessary to simulate estuarine circulation properly. This is not only true in the Chesapeake Bay, but should also be the case in many estuaries.

Acknowledgements

This work was carried out while X. Guo was visiting the Center for Coastal Physical Oceanography at Old Dominion University. He thanks support from Ministry of Education, Culture, Sports, Science and Technology, Japan. AVL acknowledges support from NSF project 9983685.

References

Austin, J.A., 2002. Estimating the mean ocean–bay exchange rate of the Chesapeake Bay. Journal of Geophysical Research 107, 3192.

Beardsley, R.C., Boicourt, W.C., 1981. On estuarine and continental shelf circulation in the Middle Atlantic Bight. In: Warren, B.A.a.C.W. (Ed.), Evolution of Physical Oceanography. The MIT Press, pp. 198–233.

Blumberg, A.F., Mellor, G.L., 1987. A description of a three-dimensional coastal ocean circulation model. In: Heaps, N. (Ed.), Three-Dimensional Coastal Ocean Models. American Geophysical Union, Washington, DC, pp. 1–16.

Boicourt, W.C., 1973. The circulation on the continental shelf from Chesapeake Bay to Cape Hatteras. Ph.D. Dissertation, The Johns Hopkins University, 183pp.

Browne, D.R., Fisher, C.W., 1988. Tide and tidal currents in the Chesapeake Bay. NOAA Technical Report NOS OMA 3, 84pp.

Chao, S.-Y., 1988a. River-forced estuarine plumes. Journal of Physical Oceanography 18, 72–88.

Chao, S.-Y., 1988b. Wind-driven motion of estuarine plumes. Journal of Physical Oceanography 18, 1144–1166.

Chao, S.-Y., 1990. Tidal modulation of estuarine plumes. Journal of Physical Oceanography 20, 1115–1123.

Chao, S.-Y., Boicourt, W.C., 1986. Onset of estuarine plumes. Journal of Physical Oceanography 16, 2137–2149.

Chapman, D.C., Lentz, S.J., 1994. Trapping of a coastal density front by the bottom boundary layer. Journal of Physical Oceanography 24, 1464–1479.

Epifanio, C.E., Garvine, R.W., 2001. Larval transport on the Atlantic continental shelf of North America: a review. Estuarine, Coastal and Shelf Science 52, 51–77.

Fong, D.A., 1998. Dynamics of freshwater plumes: observations and numerical modeling of the wind-forced response and alongshore freshwater transport. Ph.D. Dissertation, MIT-Woods Hole Oceanographic Institution, p. 172.

Garvine, R.W., 1999. Penetration of buoyant coastal discharge onto the continental shelf: a numerical model experiment. Journal of Physical Oceanography 29, 1892–1909.

Garvine, R.W., 2001. The impact of model configuration in studies of buoyant coastal discharge. Journal of Marine Research 59, 193–225.

Goodrich, D.M., Blumberg, A.F., 1991. The fortnightly mean circulation of Chesapeake Bay. Estuarine, Coastal and Shelf Science 32, 451–462.

Hanawa, K., Mitsudera, H., 1985. On daily average of oceanographic data. Coastal Oceanographic Bulletin 23, 79–87 (in Japanese).

Hargis, W.J., 1980. A benchmark multi-disciplinary study of the interaction between the Chesapeake Bay and adjacent waters. Chesapeake Bay Plume Study Superflux 1980, Williamsburg, VI, NASA Conference Publication 2188, pp. 1–14.

Isobe, A., 2005. Ballooning of river-plume bulge and its stabilization by tidal currents. Journal of Physical Oceanography 35, 2337–2351.

Kasai, A., Hill, A.E., Fujiwara, T., Simpson, J.H., 2000. Effect of the Earth's rotation on the circulation in regions of freshwater influence. Journal of Geophysical Research 105, 16961–16969.

Li, M., Zhong, L., Boicourt, W.C., 2005. Simulations of Chesapeake Bay estuary: sensitivity to turbulence mixing parameterizations and comparison with observations. Journal of Geophysical Research 110, C12004.

Marmorino, G.O., Donato, T.F., Sletten, M.A., Trump, C.L., 2000. Observations of an inshore front associated with the Chesapeake Bay outflow plume. Continental Shelf Research 20, 665–684.

McCreary, J.P., Zhang, S., Shetye, S.R., 1997. Coastal circulation driven by river outflow in a variable-density 11/2-layer model. Journal of Geophysical Research 102, 15535–15554.

Mellor, G.L., 1998. User's guide for a three-dimensional, primitive equation, numerical ocean model, Program in Atmospheric & Oceanic Sciences Report, Princeton University, 41pp.

Narayanan, C., Garvine, R.W., 2002. Large scale buoyancy driven circulation on the continental shelf. Dynamics of Atmospheres and Oceans 36, 125–152.

Nof, D., 2005. The momentum imbalance paradox revisited. Journal of Physical Oceanography 35, 1928–1939.

Nof, D., Pichevin, T., 2001. The Ballooning of outflows. Journal of Physical Oceanography 31, 3045–3058.

Oey, L.-Y., 1996. Simulation of mesoscale variability in the Gulf of Mexico: sensitivity studies, comparison with observations, and trapped wave propagation. Journal of Physical Oceanography 26, 145–175.

Pichevin, T., Nof, D., 1997. The momentum imbalance paradox. Tellus 49A, 298–319.

Pritchard, D.W., 1952. Salinity distribution and circulation in the Chesapeake Bay estuarine system. Journal of Marine Research 11, 106–123.

Pritchard, D.W., 1954. A study on the salt balance in a coastal plain estuary. Journal of Marine Research 13, 133–144.

Pritchard, D.W., 1956. The dynamic structure of a costal plain estuary. Journal of Marine Research 15, 33–42.

Reyes-Hernandez, C., 2001. Fortnightly variability in the transverse structure of density and exchange flows at the Chesapeake Bay entrance. Ph.D. Thesis, Old Dominion University, 130pp.

Seitz, R.C., 1971. Temperature and salinity distributions in vertical sections along the longitudinal axis and across the entrance of the Chesapeake Bay (April 1968–March 1969). Chesapeake Bay Institute, The Johns Hopkins University, p. 99.

Shay, L.K., Cook, T.M., Hallock, Z.R., Haus, B.K., Graber, H.C., Martinez, J., 2001. The strength of the M_2 tide at the Chesapeake Bay mouth. Journal of Physical Oceanography 31, 427–449.

Smolarkiewicz, P.K., 1984. A fully multidimensional positive definite advection transport algorithm with small implicit diffusion. Journal of Computational Physics 54, 325–362.

Spitz, Y.H., Klinck, J.M., 1998. Estimate of bottom and surface stress during a spring–neap tide cycle by dynamical assimilation of tide gauge observations in the Chesapeake Bay. Journal of Geophysical Research 103, 12761–12782.

Valle-Levinson, A., Lwiza, K.M.M., 1997. Bathymetric influences on the lower Chesapeake Bay hydrography. Journal of Marine Systems 12, 221–236.

Valle-Levinson, A., Klinck, J.M., Wheless, G.H., 1996. Inflow/outflows at the transition between a coastal plain estuary and the coastal ocean. Continental Shelf Research 16, 1819–1847.

Valle-Levinson, A., Li, C., Royer, T.C., Atkinson, L.P., 1998. Flow patterns at the Chesapeake Bay entrance. Continental Shelf Research 18, 1157–1177.

Valle-Levinson, A., Reyes, C., Sanay, R., 2003. Effects of bathymetry, friction, and rotation on estuary–ocean exchange. Journal of Physical Oceanography 33, 2375–2393.

Wang, H., Johnson, B.J., 2000. Validation and application of the second generation three dimensional hydrodynamic model of Chesapeake Bay. Water Quality and Ecosystem Modeling 1, 51–90.

Wheless, G.H., Valle-Levinson, A., 1996. A modeling study of tidally driven estuarine exchange through a narrow inlet on a sloping shelf. Journal of Geophysical Research 101, 25675–25687.

Xu, J., Chao, S.-Y., Hood, R.R., Wang, H., Boicourt, W.C., 2002. Assimilating high-resolution salinity data into a model of a partially mixed estuary. Journal of Geophysical Research 107, 3074.

Yankovsky, A.E., 2000. The cyclonic turning and propagation of buoyant coastal discharge along the shelf. Journal of Marine Research 58, 585–607.

Yankovsky, A.E., Chapman, D.C., 1997. A simple theory for the fate of buoyant coastal discharge. Journal of Physical Oceanography 27, 1386–1401.

Yankovsky, A.E., Hickey, B.M., Munchow, A.K., 2001. Impact of variable inflow on the dynamics of a coastal buoyant plume. Journal of Geophysical Research 106, 19809–19824.